

# Self-Consistent Pressure and Current Profiles in High-Beta D-<sup>3</sup>He Tokamak Reactors

Koichi UMEDA, Kozo YAMAZAKI, Tetsutarou OISHI, Hideki ARIMOTO and Tatsuo SHOJI

*Department of energy engineering and science, Nagoya University,  
Furo-cho, Chikusa-ku, Nagoya 464-8603, Japan*

(Received 8 December 2009 / Accepted 19 April 2010)

D-<sup>3</sup>He reactor has a great advantage of neutron-poor operation, but it requires higher-beta value and higher bootstrap current fraction than D-T reactor. In this paper, we investigated self-consistent plasma pressure and current profiles in the case of a positive magnetic shear mode (parabolic temperature profile) and a negative magnetic shear mode (ITB temperature profile) using TOTAL-T code including Cytran module. In a negative magnetic shear mode, toroidal beta value  $\beta_T \sim 52.4\%$  and bootstrap current fraction  $f_{bs} \sim 0.93$  was obtained in a plasma with aspect ratio 1.77, plasma major radius 6.2 m, toroidal field 4.2 T and plasma current 49.3 MA.

© 2010 The Japan Society of Plasma Science and Nuclear Fusion Research

Keywords: D-<sup>3</sup>He, negative magnetic shear, ITB, bootstrap current, high-beta value

DOI: 10.1585/pfr.5.S2030

## 1. Introduction

D-<sup>3</sup>He fusion reactor is an advanced fuel fusion reactor which does not emit neutrons from main reaction. (Neutrons are generated from the sub-reaction D-D and D-T. But the amount of neutron generation is about 1/10 of that of D-T ignition reactor). Furthermore, D-<sup>3</sup>He fusion reactors can use highly-efficient direct convertor, because the proton bears most of generation energy by the nuclear fusion reaction, and the electric conversion efficiency of 60 percent or higher are expected. Therefore, it is anticipated for following generation fusion reactor, in terms of safeness and environmental friendliness.

There are several issues in D-<sup>3</sup>He reactor. Reaction rate of D-<sup>3</sup>He is lower than that of D-T; therefore, high-beta value and high-temperature plasma is required. And in high density plasma, non-inductive current drive efficiency is very low ( $P_{CD} \propto n$ ), so high bootstrap current fraction is also needed.

First, we investigated equilibrium of arbitrary shaped core plasma of tokamak reactor, and optimized plasma parameters (aspect ratio, elongation and triangularity, etc) to obtain high-beta value plasma using APOLLO (2-D equilibrium) code [1].

Then, we simulated operation in a positive magnetic shear mode (mostly uniform current drive) and a negative magnetic shear mode (mostly off-axis current drive) with optimized plasma parameter using TOTAL (1-D Transport) code [2], and beta value, bootstrap current fraction and energy gain, etc were compared.

Here, we used the Bohm/Gyro-Bohm model in a positive magnetic shear mode [3], and used the CDBM model in a negative magnetic shear mode [4], respectively. We

coupled the CYTRAN (non-local effect of synchrotron radiation) model [5] with the TOTAL code, since synchrotron radiation loss might become dominant in high temperature operation. and used Hirshman's model for calculating bootstrap current density profile [6].

## 2. Simulation Model

### 2.1 APOLLO code (2-D Equilibrium)

Apollo equilibrium code calculates axi-symmetric equilibrium with given pressure and safety factor profiles, and solves  $n = \infty$  ideal ballooning mode equation with zero growth rate to the marginal pressure gradient and Mercier mode near the magnetic axis. The ballooning equation using a radial perturbation function  $X(s)$  through the eikonal transformation is as follows [1];

$$\frac{\partial}{\partial s} \left( A_1 \frac{\partial X}{\partial s} \right) + \frac{dp(\psi)}{d\psi} A_2 X = 0, \quad (1)$$

$$A_1 = \frac{1}{R^2 B_p} + \left( \int v' ds \right)^2 \frac{R^2 B_p^3}{B^2}, \quad (2)$$

$$A_2 = \frac{1}{B^2 B_p} \left[ 2 \frac{\partial}{\partial \psi} \left( p + \frac{B^2}{2} \right) - \frac{T B_p}{B^2} \left( \frac{\partial}{\partial s} B^2 \right) \right] \int v' ds. \quad (3)$$

Here,  $\psi$ ,  $p$ ,  $T$ ,  $J$ ,  $v'$  and  $s$  indicate poloidal flux function, plasma pressure, current stream function, Jacobian, local magnetic shear and the line element along the magnetic field line, respectively. Low- $n$  kink-ballooning modes are assumed to be stabilized by wall or mantle plasma.

The pressure profile is determined from the transport equation described in the next subsection, and the  $q$  profile is calculated from the summation of the assumed externally driven current density and the simulated bootstrap current density.

author's e-mail: yamazaki@ees.nagoya-u.ac.jp

## 2.2 TOTAL code (1-D Transport)

TOTAL code solves following equations for electron and ion density  $n_e$ ,  $n_i$ , and temperature  $T_e$ ,  $T_i$ .

$$\frac{\partial n}{\partial t} + \frac{1}{V'} \frac{\partial}{\partial \rho} V' \Gamma = S_p \quad \sum_i Z_i n_i = n_e, \quad (4)$$

$$\frac{3}{2} \frac{\partial n_i T_i}{\partial t} + \frac{1}{V'} \frac{\partial}{\partial \rho} \{V'(Q_i + \Gamma_i T_i)\} = P_i, \quad (5)$$

$$\frac{3}{2} \frac{\partial n_e T_e}{\partial t} + \frac{1}{V'} \frac{\partial}{\partial \rho} \{V'(Q_e + \Gamma_e T_e)\} = P_e, \quad (6)$$

$$\Gamma = \Gamma^{\text{NCs}} + \Gamma^{\text{NCa}} + \Gamma^{\text{AN}}, \quad (7)$$

$$\Gamma^{\text{AN}} = -D^{\text{AN}} \left\langle |\nabla \rho|^2 \right\rangle \frac{\partial n}{\partial \rho}, \quad (8)$$

$$Q = Q^{\text{NCs}} + Q^{\text{NCa}} + Q^{\text{AN}}, \quad (9)$$

$$Q^{\text{AN}} = -\chi^{\text{AN}} n \left\langle |\nabla \rho|^2 \right\rangle \frac{\partial T}{\partial \rho}. \quad (10)$$

Normalized plasma minor radius  $\rho$  and plasma volume  $V$  are defined on magnetic surface, and  $V' = dV/d\rho$ .  $\Gamma$ ,  $Q$  are particle flux and heat flux, respectively. The superscripts NCs and NCa represent contributions of axisymmetry and non-axisymmetry in neo-classical theory, and AN indicates contribution of anomalous transport.  $D$  and  $\chi$  are particle and thermal transport coefficients.  $S_p$  is particle source.  $P_i$  and  $P_e$  are ion heating power density subtracted by charge-exchange loss and electron heating power density subtracted by radiation loss, respectively

## 2.3 Anomalous transport model

As for transport coefficient, neo-classical and anomalous transport is considered separately in TOTAL code.

$$\chi = \chi^{\text{NC}} + \chi^{\text{AN}}. \quad (11)$$

Here the Chang-Hinton formula for ion transport and Hinton-Hazeltine formula for electron transport are used as neoclassical transport values as explained in Ref. [2].

### 2.3.1 Bohm/Gyro-Bohm model

Bohm/Gyro-Bohm model (14) represents H-mode transport by the addition of Gyro-Bohm model (13) to Bohm model (12) which can duplicate results of experiment in JET.

$$\chi_B = \alpha_B \frac{|\nabla P_e|}{n_e B_t} R q^2, \quad (12)$$

$$\chi_{gB} = \alpha_{gB} \sqrt{T_e} \frac{|\nabla T_e|}{B_t^2}, \quad (13)$$

$$\chi^{\text{AN}} = C_B \chi_B + C_{gB} \chi_{gB}. \quad (14)$$

Here,  $P_e$ ,  $q$  and  $B_t$  represent plasma pressure, safety factor and toroidal field, respectively. The following coefficients are used here;  $\alpha_B = 4.0 \times 10^{-5}$ ,  $\alpha_{gB} = 5.0 \times 10^{-6}$  [7].

### 2.3.2 CDBM model

The CDBM model indicates L-mode transport and ITB formation transport in a negative magnetic shear

mode.

$$\chi_{\text{AN}} = F(s, \alpha) \alpha^{3/2} \frac{c^2}{\omega_{pe}^2} \frac{v_A}{qR}, \quad (15)$$

$$s \equiv \frac{r}{q} \frac{dq}{dr}, \quad (16)$$

$$\alpha \equiv -q^2 R \frac{d\beta}{dr}. \quad (17)$$

Here,  $c$ ,  $\omega_{pe}$ ,  $v_A$ ,  $q$  and  $R$  are velocity of light, plasma frequency, Alfvén velocity, safety factor and plasma major radius, respectively. It is possible to approximate shape function  $F(s, \alpha)$  by function of  $(s-\alpha)$ , and this function decreases in the case of a weak or a negative magnetic shear, and the case of large Shafranov shift (large plasma pressure gradient).

## 2.4 Bootstrap current model

This model is obtained by solving the momentum and heat flux balance equations for electrons and ions.

$$\langle j \cdot B \rangle = L_{31} \left[ A_1^e + Z_i^{-1} T_i / T_e (A_1^i + \alpha_i A_2^i) \right] + L_{32} A_2^e, \quad (18)$$

$$L_{31} = j_0 x \left[ 0.754 + 2.21 Z_i + Z_i^2 + x (0.348 + 1.243 Z_i + Z_i^2) \right] / D(x), \quad (19)$$

$$L_{32} = -j_0 x \left[ (0.884 + 2.074 Z_i) / D(x) \right], \quad (20)$$

$$D(x) = 1.414 Z_i + Z_i^2 + x (0.754 + 2.657 Z_i + 2 Z_i^2) + x^2 (0.348 + 1.243 Z_i + Z_i^2), \quad (21)$$

$$\alpha_i = -1.172 / (1 + 0.462x), \quad (22)$$

$$x \approx (1.46 \varepsilon^{1/2} + 2.40 \varepsilon) / (1 - \varepsilon)^{1.5}. \quad (23)$$

The thermal dynamic force coefficients are  $A_1^e = P'_e / P_e$  and  $A_2^e = T'_e / T_e$ , and  $\alpha_i$  is function of the ion viscosity.  $x$  is the ratio of trapped to circulating particles.

## 3. Simulation Results

### 3.1 Critical beta values versus plasma shape

Using Apollo code, critical toroidal beta values stable against  $n = \infty$  ballooning mode is obtained as functions of plasma shape parameters (aspect ratio  $A$ , triangularity  $\delta$ ) as shown in Fig. 1. At the point of  $A < 1.8$ , critical toroidal beta increases rapidly in case of  $0.3 < \delta < 0.5$ .

As a results, we adopted the optimized plasma design parameter; aspect ratio  $A = 1.77$ , elongation  $\kappa = 2.5$ , and triangularity  $\delta = 0.5$ . In the case of toroidal field  $B_T = 4.2$  T, maximum field of coil is 20 T (current density of coil is 30 MA/m<sup>2</sup>) without breeding blanket, and the thickness of shield is assumed about 1.4 m.

### 3.2 Transport simulation in positive and negative shear

In this analysis, we obtained transient equilibrium solutions with time-varying  $q$ -profiles assuming that the current diffusive time is shorter than the plasma transport time.

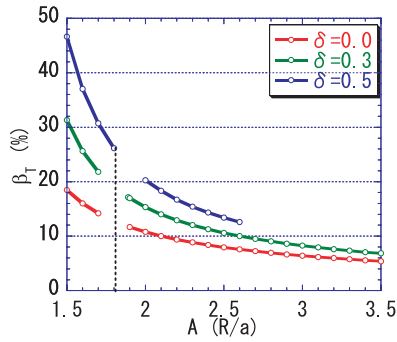


Fig. 1 Critical beta value against ballooning mode.

This does not show the exact time evolution of plasma current profile, but finally we can obtain the exact quasi-stationary equilibrium.

In the burning control algorithm to get ignition, low density plasma with high external heating power is initially assumed, and the density is gradually raised with decreasing external heating power to get the target ignition state. In this analysis, the external heating power density profile is assumed parabolic, and the particle source  $S_p$  is automatically introduced to get target average density. As boundary conditions in the present typical analysis, edge density and edge temperature are fixed to  $2 \times 10^{19} \text{ m}^{-3}$  and 1 keV, respectively.

The transport process is nonlinear, but no bifurcated states might exist in the thermally stable regime in burning plasmas. If the input parameters in the unstable regime, such as high-density low-temperature regime, are adopted, the transport analysis cannot reach to the ignition state.

In the case of a positive magnetic shear (Fig. 2), we obtain parabolic temperature profile (b), and nearly constant bootstrap current density profile (a) except area at the center and the edge. At the center, temperature gradient becomes  $\sim 0$ ; as a result, bootstrap current disappears and then current drive becomes essential. This situation is same in other two (negative magnetic shear modes) simulation cases. On the other hand, at the edge, temperature gradient becomes sharp (ETB), thereby bootstrap current density becomes high.

In the case of a negative magnetic shear mode, internal transport barrier was formed at the point of slightly outside of  $q' = 0$ , (Fig. 3, Fig. 4), and temperature, density and toroidal beta value became higher than those of a positive magnetic shear mode. (Fig. 2 (b), Fig. 3 (b), Fig. 4 (b)). The larger bootstrap current flows at the point of large pressure gradient, and the pressure gradient becomes larger at the point of the large plasma current density. As a results, operation that bootstrap current fraction is very high (current are driven only at the center of plasma) is maintainable. (Fig. 3 (a)).

Figure 4 shows a simulation result with external current driven at the edge ( $r/a \sim 0.6$ , slightly outside of  $q' = 0$ ) in addition to at the center. In this case, the ITB foot

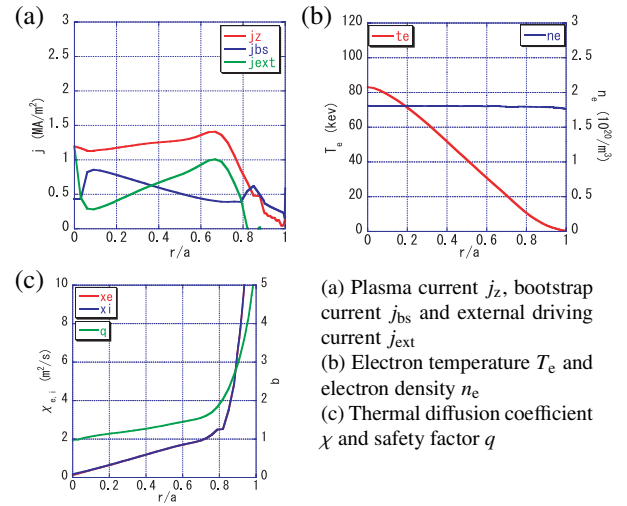


Fig. 2 Radial profiles in a positive magnetic shear mode. (External current with flat profile is assumed.)

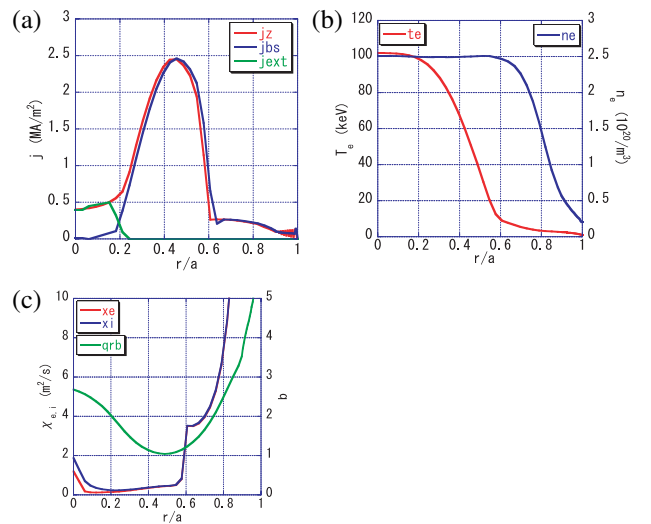


Fig. 3 Radial profiles in a strong negative magnetic shear mode. (External current is driven at the center.)

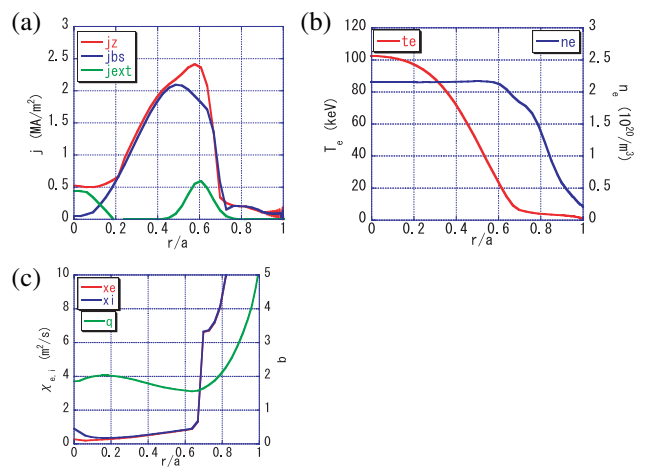


Fig. 4 Radial profiles in a weak negative magnetic shear mode. (External current is driven at the center and the surrounding part  $r/a \sim 0.6$ .)

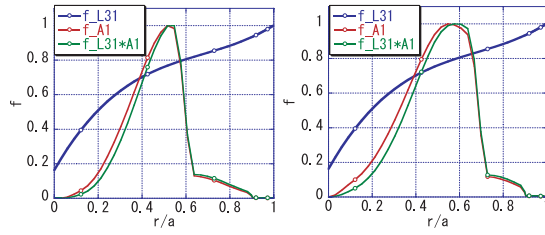


Fig. 5 Radial profiles of factors for bootstrap current calculation normalized  $A_1 = P'_\alpha/P_\alpha$ ,  $L_{31}$  (Eq. 19) and  $A_1L_{31}$ .

point shifts outwards compared with no edge current drive case ( $r/a: 0.6 \Rightarrow 0.7$ ) (Fig. 3 (b), Fig. 4 (b)). Therefore, in a weak negative magnetic shear mode, higher fusion power and higher  $\beta$  value operation will be possible.

In a strong negative magnetic shear mode, initial rise of temperature becomes more steep than that of in a weak negative magnetic shear mode (Fig. 3, Fig. 4), and plasma pressure gradient  $A_1$  becomes more sharp (Fig. 5). And a coefficient  $L_{31}$  (Eq. 19) is roughly same profile, and increases gradually from  $r/a = 0.4$  to the edge. Since bootstrap current density is proportional to  $L_{31} \times A_1$ , in a strong magnetic shear mode, plasma pressure profile has a strong consistency for bootstrap current density profile. As a result, current drive power in a strong magnetic shear mode is small, and off-axis current drive is required in a weak negative magnetic shear mode.

A summary output of three designs is shown in Table 1. In a positive magnetic shear mode, about 1 GW current drive power is required, therefore reactor might not be realized. In D-<sup>3</sup>He reactor, that requires high fuel density, but non-inductive current drive power becomes high ( $P_{cd} \propto n$ ). It's important to have a balance between beta value and energy gain.

## 4. Conclusion

For realizing high-beta low aspect ratio D-<sup>3</sup>He reactor stable against high-n ballooning mode, plasma configurations with aspect ratio  $A \leq 1.8$ , elongation  $\kappa = 2.5$  and triangularity  $0.3 < \delta \leq 0.5$  are preferable.

Table 1 Summary output.

	Strong negative shear	Weak negative shear	Positive shear
$P_{fus}$ (MW)	3440	3688	3510
$I_r$ (MA)	49.3	62.6	62.3
$I_{bs}$ (MA)	46.8	55.1	32.3
$f_{bs}$	0.93	0.88	0.52
$P_{cd}$ (MW)	143	279	1116
$P_H$ (MW)	40.0	41.6	45.3
$T_e(0)$ (keV)	102	102	83.1
$[T_e]$ (keV)	35.6	39.2	30.6
$\langle n \rangle$ ( $10^{20}/m^3$ )	1.97	1.80	1.80
$\beta_T$ (%)	52.4	54.7	35.6
$HH_{Bohm,CDBM}$	1.5	1.5	3.0
$\tau_E$ (s)	4.67	4.53	4.68
$Q$	18.8	11.5	3.0

Negative magnetic shear modes have great advantages in terms of fusion power, bootstrap current fraction and other plasma parameters in D-<sup>3</sup>He reactor, compared with a positive magnetic shear mode case.

High bootstrap current fraction is accomplished in a strong magnetic shear.

Externally Driven current at the edge in addition to at the center (a weak negative shear mode) raises  $P_{fusion}$ , but decreases  $Q$  value. ( $\beta_T: 52.4\% \Rightarrow 54.7\%$ ,  $P_{fusion}: 3440 \text{ MW} \Rightarrow 3688 \text{ MW}$ ,  $Q: 18.8 \Rightarrow 11.5$ )

- [1] K. Yamazaki, T. Amano, H. Naitou, Y. Hamada and M. Azumi, Nucl. Fusion **25**, 1543 (1985).
- [2] K. Yamazaki and T. Amano, Nucl. Fusion **32**, 633 (1992).
- [3] M. Erba, A. Cherubini, V. V. Parail, E. Springmann and A. Taroni, Plasma Phys. **39**, 261 (1997).
- [4] K. Itoh, *et al.*, Plasma Phys. Control. Fusion **35**, 543 (1993).
- [5] F. Albajar, M. Bornatici and F. Engelmann, Nucl. Fusion **42**, 670 (2002).
- [6] S. P. Hirshman, Phys. Fluids **31**, 10 (1988).
- [7] M. Erba, A. Cherubini, V. V. Parail, E. Springmann and A. Taroni, Plasma Phys. Control. Fusion **39**, 261 (1997).